The p - d hybridization in the electronic structure of α-Ag_2Te

1997 J. Phys.: Condens. Matter 9 6031

(http://iopscience.iop.org/0953-8984/9/28/003)

J. Phys.: Condens. Matter **9** (1997) 6031–6048. Printed in the UK PII: S0953-8984(97)76643-8

The p–d hybridization in the electronic structure of α-Ag_2Te

H Kikuchi†, H Iyetomi‡ and A Hasegawa‡

† Graduate School of Science and Technology, Niigata University, Ikarashi, Niigata 950-21, Japan

‡ Department of Physics, Niigata University, Ikarashi, Niigata 950-21, Japan

Received 24 July 1996, in final form 18 March 1997

Abstract. The electronic structure of α-Ag_2Te is discussed, with special attention paid to possible roles of the p–d hybridization, on the basis of density functional calculations in the local-density approximation; α-Ag_2Te is a typical superionic conductor, and also exhibits interesting electronic properties. Fully self-consistent calculations based on the energy variational principle are carried out for a hypothetical crystalline compound, Ag_2Te with the antifluorite structure, making use of the linearized augmented-plane-wave method. The calculated equilibrium lattice constant agrees with a measured value within an accuracy of 5%. The self-consistent determination of the relative sizes of the augmented-plane-wave spheres leads to an energy band structure similar to that of a narrow-gap semiconductor, in accordance with experiments. Also, the magnitudes predicted for the effective masses of the electrons and holes are almost within the experimental uncertainties. Such quantitative agreement even with the static model arises from the following facts: (i) the Ag d states and the Te p states are not hybridized to such an extent as to have a significant influence on the band-structure characteristics near the energy gap; and (ii) the lowest conduction band consists mainly of Ag and Te s states with extended character. Thus the p–d hybridization can hardly be considered to be the mechanism that induces the superionic conductivity in α-Ag_2Te.

1. Introduction

The superionic conductors have attracted much academic and also technological interest, since these materials exhibit substantial ionic conductivity, comparable to that for liquid electrolytes, at relatively low temperatures. The silver chalcogenides Ag_2X (X represents S, Se, or Te) in their α-phases are well known as typical superionic conductors [1–6]. In the α-phases, the chalcogen ions form simple sublattices, while the Ag ions are located in and move through characteristic voids in the sublattices; the regularity of the crystalline lattice is thus significantly broken up.

To elucidate the peculiar ion dynamics in the superionic conductors, extensive molecular dynamics simulations have been carried out using interatomic potential functions, which were determined in phenomenological ways [7–9]. These studies have quantitatively succeeded well in explaining the partial melting of Ag ions and the onset of the fast-ionic transport with increased temperature. However, there are no first-principles explanations for why Ag ions show particularly large diffusivity in the chalcogen matrices as compared with the other noble-metal and alkaline ions. For a deeper understanding of such fascinating properties, therefore, it is indispensable to clarify the microscopic role of electrons in determining the potential functions for the ionic motion.

0953-8984/97/286031+18$19.50

The possibility of hybridization between the Ag 4d states and the p states of the atoms forming the sublattices is one of the key issues in uncovering the interrelationship between the ion dynamics and the electronic structures in the superionic conductors; the Ag d states with the energy of −0.60 Ryd lie just below the p states with the energies of −0.53 Ryd (sulphur), −0.50 Ryd (selenium), −0.46 Ryd (tellurium), and −0.54 Ryd (iodine) considered as individual atoms. For silver iodide, another typical superionic conductor, the electronic structures have been studied by combining photoelectron data with results from x-ray and UV spectroscopy, and compared with those of the other silver halides such as AgCl and AgBr [10–15]; for silver chalcogenides, however, only limited experimental data are available [16]. The upper valence band in AgI was shown to consist predominantly of p states which originated from the iodine 5p states. Also, there is appreciable overlap between the Ag d states and the halogen p states in the densities of states. Before and after the superionic phase transition, the overall shapes of the partial p and d densities of states do not significantly alter except for a small change in the total width of the p density of states. Such experimental observation led Fedorin [17] to propose that the selective substantial diffusivity of silver ions arose from strong hybridization between the d states of silver and the p states of halogen or chalcogen atoms; more detailed modelling was later given [18] for the superionic transition in the silver halides.

Silver chalcogenides are characterized as narrow-gap semiconductors in addition to being superionic conductors, and exhibit various interesting electronic properties, such as substantial carrier mobility, and enhanced infrared absorption as compared with that of the halogen counterparts. Electrical, optical, and electrochemical measurements [19–21] suggest that the electronic structure of α-Ag_2Te is similar to that of a semiconductor with a narrow energy band gap [19, 20]. The energy band gap is experimentally determined as 0.007 Ryd (0.1 eV). The effective masses of the electron carriers are very small, i.e., they are in the range from $0.050m_0$ to $0.069m_0$, with m_0 the free-electron mass, while the effective masses of the hole carriers are much larger than the electron effective masses, i.e., in the range from $1.0m_0$ to $2.0m_0$ [19, 20]. An appreciable deviation from a parabolic energy band structure in the vicinity of the bottom of the conduction band has been confirmed experimentally also. Similar electronic structures have been observed for the other two Ag chalcogenides [21].

To shed light on the electronic structures observed for the Ag chalcogenides, including α-Ag_2Te, one of the present authors [22] has carried out augmented-plane-wave (APW) calculations for some hypothetical crystalline compounds. In superionic conductors, the Ag ions, being mobile, are expected to move far more slowly than the electrons. In fact, the ratio of the mobility of the Ag ions to that of the electrons is found by measurement to be around 10^{-6} for α-Ag_2Te. Such a large difference in mobilities gives rise to an intuitive view that the electrons in α-Ag_2Te may 'feel' as if the Ag ions were frozen at certain locations in the FCC Te lattice. As a result of the calculations based on this intuition, semiquantitative agreement between theory and experiment was obtained for the energy gap and the effective masses. It was then suggested that the strong hybridization of the Ag 5s band and the Te 6s band is the origin of the smallness of the electron effective mass. The hybridization of the Ag 4d band and the Te 5p band was also indicated as affecting the magnitude of the hole effective mass and the energy band gap. It was thus concluded that the energy band structure near the energy gap depended sensitively on these s–s and p–d hybridization effects. However, the calculations, which used experimental lattice constants and *ad hoc* Kohn–Sham potentials, were not carried out in a self-consistent way. The choice of the sizes of the APW spheres also remains an open question; equi-radial spheres were used in the previous calculations. As will be appreciated, in fact, the sphere size sensitively controls the

electronic band structure near the Fermi level. The conclusions are thus provisional in this sense.

In this paper we extend the theoretical analysis for the electronic structure in α-Ag_2Te, along the lines laid down by one of the authors, with the aim of achieving a microscopic understanding of the mechanism of the superionic conductivity, and also for the purpose of explaining various electronic properties observed experimentally. We reconsider the previous results for Ag_2Te with the hypothetical crystalline structure by carrying out *fully self-consistent* calculations in the framework of the density functional theory with the local-density approximation. We take α-Ag_2Te as the target system, because the deviation from the regularity of the crystalline structure is less significant for this system than for the other two Ag chalcogenides. The ground-state properties, such as the cohesive energy and the bulk modulus, are calculated at an equilibrium lattice constant determined through minimization of the total energy. The Kohn–Sham equation is solved iteratively, to achieve self-consistency of the solution. We also determine the radii of the APW spheres according to the variational principle. The energy band gap and the effective masses of the conduction and valence bands are then calculated at the lattice constant in equilibrium, and compared with available experimental results. Detailed analyses of the characteristics of the energy bands are also performed.

Accumulating the results obtained here, we can examine the validity of the conclusions given in the previous study on a sounder theoretical basis. In the previous calculations, reduction of the p–d hybridization achieved by selectively shifting the Ag d band was essential to explaining the semiconducting band structure for α-Ag_2Te. Here, however, we demonstrate that the self-consistent determination of the sizes of the APW spheres provides a clue as regards how to reproduce such electronic structure. We thus find that the reduced p–d hybridization is naturally realized by imposing self-consistency on the theoretical calculations; the present calculations are thereby carried out using optimized parameters which are determined by minimization of the total energy. Eventually the Ag d band and the Te p band are so separated that the band-structure characteristics near the Fermi level are insensitively controlled by the extent of the p–d hybridization. The p-band characteristics, such as the hole effective mass and the band width, are simply determined by the increase in the overlapping of the neighbouring Te p states, which is promoted by Ag atoms.

The organization of this paper is as follows. The computational procedure for obtaining the energy band structure based on a linearized APW method is described in section 2. In section 3, results for the ground-state properties and the electronic band structure of Ag_2Te with the hypothetical crystalline structure are given. The energy band structure for the pure FCC Te lattice is also presented as a reference. In section 4, the features of the electronic structure deduced from the present calculations are discussed with reference to the results obtained previously. Concluding remarks are given in section 5.

2. Methods

In the observed structure of α-Ag_2Te, the Te ions form a FCC lattice with the lattice constant $a = 6.576$ Å at 523 K. The Ag ions, on the other hand, are distributed dominantly among sites of two crystallographically different types, i.e., tetrahedral 8c and octahedral 4b sites, in the Te lattice [23, 24]. Since the crystallographical measurements suggest that the Ag ions distribute around the 8c sites with appreciably greater probability than around the octahedral sites, we here assume that they are located stoichiometrically at the 8c sites in the Te lattice. Such an arrangement of the Ag and Te ions forms the antifluorite crystal structure which

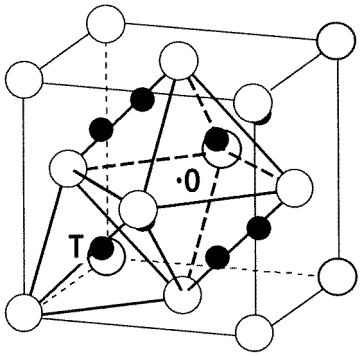

Figure 1. The antifluorite structure. White spheres: Te atoms; black spheres: Ag atoms. The antifluorite structure consists of two kinds of polyhedron: tetrahedra and octahedra. The points T and O denote the 8c sites (tetrahedral sites) and the 4b sites (octahedral sites), respectively.

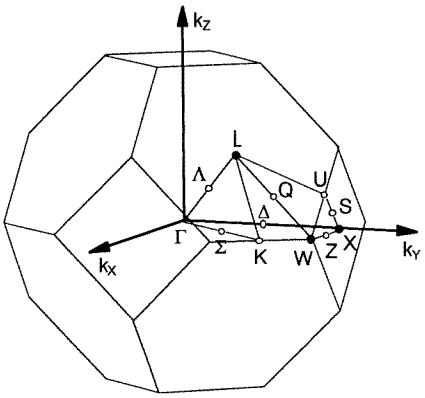

Figure 2. The Brillouin zone and an irreducible 1/48 part for the FCC Bravais lattice.

is shown in figure 1. It contains one molecule of Ag_2Te per primitive cell, and has the space group $Fm3m$. The first Brillouin zone corresponding to the antifluorite structure is shown in figure 2, with typical symmetric points labelled in its irreducible 1/48 part. This hypothetical crystalline compound will hereafter be referred to simply as Ag_2Te.

The ground-state properties of the electrons are calculated for Ag_2Te in the framework of the density functional theory (DFT) with the local-density approximation (LDA) [25–29], where the paramagnetic state is assumed. For the functional form of the exchange and correlation energy, we use the parametrization given by Janak, Moruzzi and Williams [30]. The Kohn–Sham equation for the one-electron states is then solved self-consistently by means of the linearized augmented-plane-wave (LAPW) method [31–33]; we employ the linearization scheme proposed in [33]. The charge-density distribution and the Kohn–Sham potential are calculated [34] in the muffin-tin approximation (MTA). The DFT with the LDA, which we have adopted here, is known to yield good results in practice [35, 36] for the electronic structure of a wide variety of materials, even though the DFT itself is designed to conform to the ground-state total energy and the electron density distribution, and not to the electronic structure.

The crystal data for the hypothetical compound used in the present calculations are listed

Table 1. Crystal data for the hypothetical compound Ag_2Te.

Crystal structure		Antifluorite type
Space group		$Fm3m$
Lattice constant	a_0	6.801 Å (=12.852 22 au)
Atomic positions	Te	(0, 0, 0)
	Ag	(1/4, 1/4, 1/4)
		(1/4, 1/4, 3/4)
	Empty sphere	(1/2, 1/2, 1/2)
APW sphere radii	R(Te)	0.236 18 a_0 (=3.035 44 au)
	R(Ag)	0.196 82 a_0 (=2.529 57 au)
	R(empty)	0.236 18 a_0 (=3.035 44 au)

in table 1. The lattice constant a_0 is a theoretical value post-determined by minimizing the total energy. The numerical procedure for imposing the equilibrium condition on the energy will be described in the next section. Empty APW spheres are placed at the octahedral sites in addition to the APW spheres at the atomic sites [37]. The introduction of the empty spheres may improve the accuracy of the APW calculations for a compound with open structure, such as that studied here; in fact it does, as will be shown later.

As for the radii of the APW spheres, there is no definite prescription as regards how to choose them. As usual, we select the spheres to be as large as possible, without overlapping each other. The relative sizes of the spheres, however, remain undetermined. To fix these free parameters, we employ the energy variational principle; that is, we minimize the total energy by varying the radii of the Te, Ag, and empty APW spheres for a given lattice constant. Then the total energy so obtained is minimized as a function of the lattice constant. Details of the variational scheme for the APW spheres, and the improvement in the APW calculations that arises for ionic compounds, will be published elsewhere [38]. The *variational* determination of the APW spheres is indispensable to reproducing the semiconducting nature of α-Ag_2Te here, and the electronic structure near the Fermi level is shown to be sensitive to the choice of the APW sphere radii. As a result of such optimization, the Te, Ag, and empty APW sphere radii have been determined as $0.2362a_0$, $0.1968a_0$, and $0.2362a_0$, respectively, at the equilibrium lattice constant $a_0 = 6.801$ Å. The APW spheres at the Te, Ag, and empty sites, and the interstitial region eventually occupy 19.5%, 29.5%, 19.5%, and 31.5% of the total space in the crystal, respectively. The packing ratio, 68.5%, is comparable to those for close-packed structures, 74% (FCC) and 68% (BCC), for which the MTA works well.

The iteration process for solving the Kohn–Sham equations starts with a crystal charge density constructed by superposing the atomic charge densities for the neutral atoms Te (Kr, $4d^{10}5s^25p^4$) and Ag (Kr, $4d^{10}5s^1$), where Kr stands for the electronic configuration of krypton. The atomic states are also obtained by solving the Kohn–Sham equation within the LDA. The Kr core plus the $4d^{10}$ states for Te and the Kr core for Ag are assumed to be unchanged during the iteration; i.e., the frozen-core approximation is adopted in the crystalline calculations.

The crystal charge densities are constructed by taking 19 sampling $\boldsymbol{k}$-points which are uniformly distributed in the irreducible 1/48 part of the Brillouin zone as shown in figure 2. At each $\boldsymbol{k}$, about 460 LAPW basis functions are employed under the condition $|\boldsymbol{k} + \boldsymbol{K}_n| \leqslant 7.5(2\pi/a_0)$, where the $\boldsymbol{K}_n$ are reciprocal-lattice vectors, and the angular momenta up to $l = 8$ are taken into account. These conditions, for which the total energy converges well within a few mRyd, are found by changing various parameters such

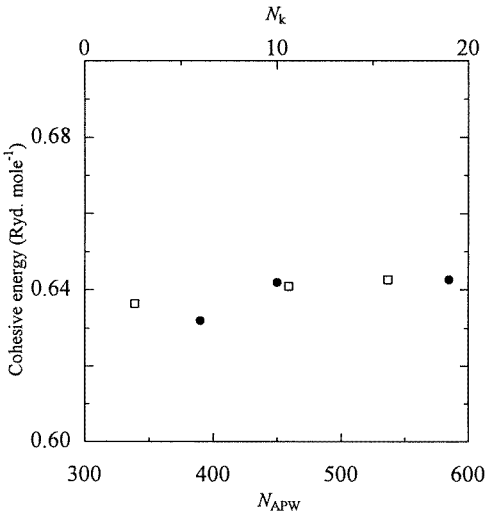

Figure 3. A convergence test for the cohesive energy calculated with the lattice constant set at 6.800 Å for the APW sphere radii $0.236\,18a_0$ (Te), $0.196\,82a_0$ (Ag), and $0.236\,18a_0$ (empty site). The open squares show a series of results for which N_{APW} varies, with $N_k = 19$. The full circles show results for which N_k varies, with $N_{APW} = 537$.

as the number of sampling $\boldsymbol{k}$-points, $N_{\boldsymbol{k}}$, the number of basis functions, N_{APW}, and the maximum angular momentum, l_{max}. An example of the test for the convergence of the total energy is shown in figure 3. The convergence criterion for the self-consistency is given by $\max |rV_{in}(r) - rV_{out}(r)| \leqslant 0.001$, where $V_{in}(r)$ and $V_{out}(r)$ denote the input and output Kohn–Sham potentials, respectively.

To derive the density of states, the energy eigenvalues are calculated at 489 $\boldsymbol{k}$-points, including a number of general $\boldsymbol{k}$-points, in the irreducible 1/48 part of the Brillouin zone, using the final self-consistent potential. To compare with the experimental results, the density of states $D(E)$ is calculated as a function of the energy E by summing over a Lorentzian which has linewidth τ and is centred at each energy eigenvalue ϵ_i:

$$D(E) = \sum_i \frac{\tau/\pi}{(E-\epsilon_i)^2 + \tau^2}. \tag{1}$$

The Fermi energy E_F is determined from

$$N_e = \int_{-\infty}^{E_F} D(E)\ \mathrm{d}E \tag{2}$$

where N_e is the total number of electrons.

3. Results

3.1. Ground-state properties

Firstly, in order to obtain the ground state of the Ag_2Te, the total energy E (per molecule) is calculated for five values of the lattice constant a in the range from 6.400 Å to 7.200 Å; the results are plotted in figure 4. Then, the calculated results are fitted to the equation of state proposed by Murnaghan [41] by the method of least-squares fitting. As is shown in

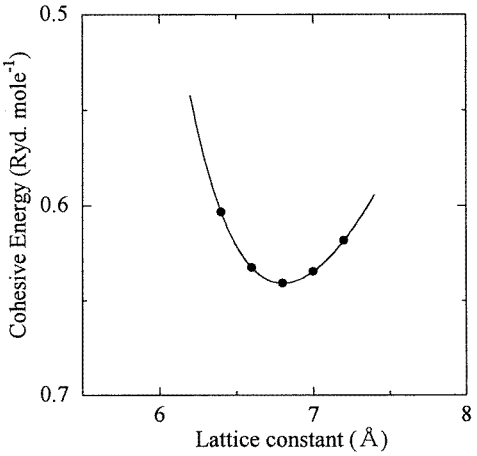

Figure 4. The total energy, measured relative to the atomic energy E_{atom}, for Ag_2Te, as a function of the lattice constant calculated with the optimized APW sphere radii. The dots and the solid curve show the original numerical values and the analytic results fitted to the Murnaghan formula, respectively.

figure 4, the total energy fitted by the equation of state can interpolate the calculated results very precisely. The minimum of the total energy E_{min} is calculated using the equation of state, and it determines the ground-state properties, such as the equilibrium lattice constant a_0, the cohesive energy E_{coh}, and the bulk modulus B_0. The cohesive energy is defined as the difference between E_{min} and E_{atom}, i.e., $E_{coh} = E_{atom} - E_{min}$. Note that the zero-point vibration energy is neglected in the total energy for the crystal.

Table 2. The theoretical results for the ground-state properties of the hypothetical crystalline compound Ag_2Te, compared with the available experimental results at 523 K for α-Ag_2Te.

	Lattice constant (Å)	Cohesive energy (Ryd mol^{-1})	Bulk modulus (GPa)
Calculation	6.801	0.6409	50.4
Experiment	6.576 [23]	——	18.9 [39]

In table 2, the results thus calculated for a_0, E_{coh}, and B_0 are listed, together with the experimental results for a_0 and B_0 which were measured at 523 K for α-Ag_2Te. We note that the calculated values should be compared with values of the experimental results extrapolated to 0 K. The lattice constant so extrapolated, with the thermal expansion coefficient measured experimentally, is 6.455 Å, which is predicted by the theoretical calculations with an accuracy of 5%. Since the temperature dependence of the bulk modulus is not available experimentally, we cannot estimate a value which can be compared with the calculated one; the experimental data show that both Young's modulus and the shear modulus strongly depend on the temperature [42]. The cohesive energy has been measured neither for α-Ag_2Te nor for the other two Ag chalcogenides, as far as we know. In passing, we remark here that the empty APW spheres at the octahedral sites work well as regards predicting the lattice constant. Without these spheres, the lattice constant is calculated as 7.377 Å, which is significantly larger than the experimental value.

3.2. Electronic energy band structure at the equilibrium

We first calculate the energy band structure for the pure FCC Te lattice with a lattice constant identical to that of the Ag_2Te lattice. Then, we calculate the energy band structure for Ag_2Te with the antifluorite structure, and compare the two results to elucidate the effects of the Ag ions on the electronic structure in the Ag_2Te.

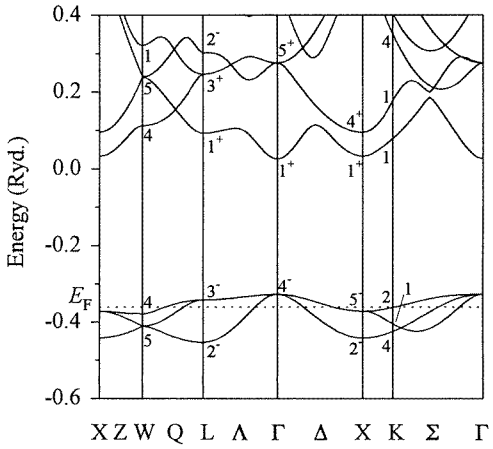

Figure 5. The energy band structure calculated for the pure FCC Te lattice at the equilibrium lattice constant of the Ag_2Te. Bethe's notation is used for the irreducible representations. E_F indicates the Fermi energy.

3.2.1. The FCC Te lattice without Ag atoms. The energy band structure along the high-symmetry directions in the Brillouin zone is shown in figure 5. For irreducible representations of space groups, the symmetry labels due to Bethe are used here. The three bands which lie in the energy range between -0.5 Ryd and -0.3 Ryd consist dominantly of the p state, which originates from the Te 5p state. The band which lies in the energy range between 0.0 Ryd and 0.1 Ryd consists dominantly of the s state, which originates from the Te 6s state. The bottom of the s band is located at the Γ point. The p bands are separated from the s band by a large energy gap. The Fermi level E_F is located at -0.361 Ryd, and is indicated by a dotted line in figure 5. The narrow band which lies at about -1.0 Ryd originates from the Te 5s state, and is omitted from figure 5. The energy band structure shown in figure 5 is that of a metal.

Table 3. Various characteristic energies in the electronic band structure for the Ag_2Te. The energies are in Ryd.

	Present work	Experiment
Band gap at the Γ point	0.015	0.009 [20]
p-like band width	0.362	——
d-like band width	0.133	——
Fermi level	0.244	——

The following simplified argument concerning the doping effects of the Ag atoms begins by regarding this energy band structure as that of a semiconductor. Suppose that each Ag

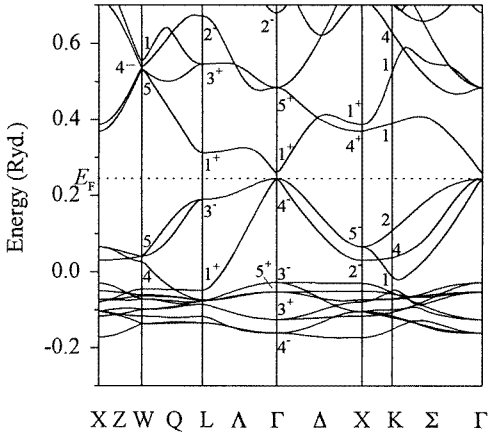

Figure 6. The energy band structure calculated for the Ag_2Te with the antifluorite structure at the equilibrium lattice constant. Bethe's notation is used for the irreducible representations. E_F indicates the Fermi energy.

atom only supplies one 5s electron, without any disturbance of the one-electron potential, when two Ag atoms are put into each primitive cell of this FCC Te lattice. The p bands thus become fully occupied, and are regarded as the valence band, which is separated from the conduction band by a large energy band gap. The top of the valence band is the Γ_4^- state, and the bottom of the conduction band is the Γ_1^+ state. The energy band gap is thus direct, and its magnitude is 0.35 Ryd. The effective mass is very nearly isotropic at the bottom of the conduction band, and its mean value is $0.3m_0$. The valence band top consists of triply degenerate states, and the effective mass in the uppermost band in the vicinity of the top is $7.6m_0$ on average. These results are in good agreement with the previous calculation [22]. We will show in the next section how such 'semiconducting' characteristics of the pure Te crystal are modified by the actual doping of the Ag atoms.

3.2.2. Ag_2Te with the antifluorite structure. The energy band structure for the Ag_2Te along the high-symmetry directions in the Brillouin zone is shown in figure 6. A narrow band which originates from the Te 5s state lies at around -0.52 Ryd, and is omitted from figure 6. The Fermi level is located at 0.244 Ryd, and is indicated by a dotted line in figure 6. It coincides with the Γ_4^- state at the top of the valence band. The Γ_1^+ state is located at the bottom of the conduction band. The band-structure characteristics are listed in table 3. The energy band structure of this hypothetical compound turns out to be that of a narrow-gap semiconductor, in agreement with experiments.

A semiconducting band structure with a large energy gap is obtained for FCC Te; the stoichiometric addition of the Ag atoms into the FCC Te lattice is found to affect this band structure drastically. The bottom of the conduction band (Γ_1^+) is lowered as compared with the X_1^+ state, while the p bands in the valence band become wider, and the valence band top is raised. The Fermi energy increases from -0.361 Ryd to 0.244 Ryd. As a result, the magnitude of the energy band gap is much reduced.

In order to investigate the characteristics of each band, the position probability densities for the Bloch electrons were calculated, and their distributions were partitioned according to the sites (the Te and Ag sites, the empty APW spheres, and the interstitial region) and the angular momenta (defined only inside the APW spheres). The results for the partial

Table 4. The distribution (expressed as percentages) of the position probability functions, partitioned according to the sites and the angular momenta for the Bloch states at the Γ, X, and L points.

Band index	Bloch state	Energy (Ryd)	Interstitial region	Te spheres				Ag spheres				Empty spheres			
				s	p	d	f	s	p	d	f	s	p	d	f
Γ point															
1	Γ_4^-	−0.161	10	0	17	0	0	0	0	69	0	0	3	0	0
2	Γ_3^+	−0.125	10	0	0	1	0	0	0	87	0	0	0	1	0
3	Γ_5^+	−0.053	3	0	0	1	0	0	0	96	0	0	0	0	0
4	Γ_3^-	−0.029	3	0	0	0	0	0	0	97	0	0	0	0	0
5	Γ_4^-	0.244	9	0	60	0	0	0	3	26	0	0	0	0	1
6	Γ_1^+	0.259	24	26	0	0	0	25	0	0	0	25	0	0	0
7	Γ_5^+	0.484	44	0	0	19	0	0	28	0	1	0	0	8	0
X point															
1	X_2^-	−0.172	23	0	26	0	0	12	0	35	0	0	5	0	0
2	X_4^-	−0.116	9	0	0	0	1	0	0	89	0	0	0	0	1
3	X_4^+	−0.104	10	0	0	1	0	2	0	86	0	0	0	1	0
4	X_5^-	−0.104	7	0	15	0	0	0	1	76	0	0	0	0	1
5	X_1^+	−0.079	8	4	0	1	0	0	1	79	0	6	0	0	0
6	X_5^+	−0.073	4	0	0	2	0	0	0	93	0	0	0	1	0
7	X_3^-	−0.051	3	0	0	0	1	0	0	96	0	0	0	0	0
8	X_2^+	−0.030	3	0	0	0	0	0	0	97	0	0	0	0	0
9	X_2^-	0.031	9	0	19	0	0	8	0	61	0	0	2	0	0
10	X_5^-	0.066	22	0	44	0	0	0	9	17	0	0	7	0	0
11	X_4^+	0.369	28	0	0	14	0	41	0	10	0	0	0	6	0
12	X_1^+	0.387	27	7	0	8	0	0	12	12	0	34	0	0	0
L point															
1	L_3^-	−0.134	10	0	18	0	0	0	1	69	0	0	0	1	0
2	L_2^-	−0.117	26	0	34	0	0	12	4	12	0	11	0	0	0
3	L_3^+	−0.085	8	0	0	1	0	0	0	90	0	0	1	0	0
4	L_3^-	−0.077	6	0	0	0	1	0	0	92	0	0	0	1	0
5	L_3^+	−0.077	5	0	0	2	0	0	0	92	0	0	1	0	0
6	L_2^-	−0.074	7	0	9	0	1	2	0	80	0	0	0	1	0
7	L_1^+	−0.049	5	2	0	1	0	1	0	89	0	0	1	0	1
8	L_3^-	0.190	12	0	52	0	0	0	5	28	0	0	0	2	0
9	L_1^+	0.312	30	12	0	7	0	34	1	3	1	0	10	0	1
10	L_3^+	0.546	36	0	0	18	0	0	20	8	0	0	17	0	1

contributions (as percentages) at the Γ, X, and L points are listed in table 4.

The three valence bands that lie between −0.05 Ryd and E_F originate dominantly from the Te 5p states. The ten bands that appear just below these three p bands consist dominantly of Ag 4d states. We see that the Ag d bands are 'spatially' well separated from the Te p

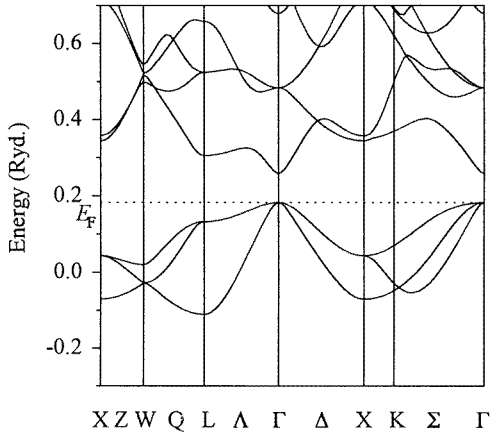

Figure 7. As figure 6, but recalculated after lowering the Ag d band by 0.3 Ryd, using the self-consistent Kohn–Sham potentials.

bands, in view of the fact that the energy levels of these atomic orbitals are very close. Hybridization, however, occurs between the two states to some extent. For example, in the lowest d band, the Te p component and the Ag d component amount to 17% and 69% of the total charge at the Γ point, 26% and 35% at the X point, and 18% and 69% at the L point, respectively. To elucidate the effects of such p–d hybridization on the electronic structure, we have repeated the same calculation, but artificially lowering the location of the d band by 0.3 Ryd, as shown in figure 7. The procedure for shifting the d band which was employed in [22] solely varies the resonance condition of the Ag d states to control the extent of hybridization between the Ag d states and others. We observe no significant change in the electronic structure, especially near the Fermi level. We can therefore refer to the relationship between the Ag d states and the Te p states as being weakly hybridized. This is also established quantitatively in the next section, on effective masses.

In the vicinity of the conduction band bottom, the Bloch state consists dominantly of the Ag s component, but also contains an appreciable contribution from the Te s component. Thus, the energy of the Γ_1^+ state can vary sensitively with the Ag s–Te s hybridization. The unoccupied Te 5d states form rather complicated bands in the upper part of the s band.

The partial charge distributions in each APW sphere and in the interstitial region for the Ag_2Te are listed in table 5. The charge-transfer rates may be defined as the differences between the charge distributions and those resulting from the superposition of the atomic charge densities, and are listed in table 5 also. The valence charge is found to be transferred from the Ag APW sphere to the Te APW sphere. The net charge contained in the Ag APW sphere is $+1.29e$. Note that this is considerably larger than the effective charge ($+0.55e$) for Ag ions commonly used in molecular dynamics calculations [43, 44].

3.3. Effective masses

On the basis of a simple effective-mass approximation, the effective masses of the electron carriers are derived from the energy band structure along the high-symmetry axes around the conduction band bottom. The effective mass averaged over the three high-symmetry axes is $m_e^* = 0.039m_0$. The effective masses of the hole carriers are derived from the energy band structure around the top of the uppermost valence band, and likewise averaged over

Table 5. The numbers of valence electrons contained in the Te, Ag, empty APW spheres, and interstitial region. The numbers in the APW spheres are decomposed into partial contributions according to the angular momenta.

	Te APW sphere					Ag APW sphere				
	s	p	d	f	Total	s	p	d	f	Total
Atomic superposed	2.05	2.77	0.21	0.00	5.03	0.38	0.16	9.33	0.00	9.87
Self-consistent	1.68	3.32	0.15	0.05	5.20	0.25	0.19	9.26	0.01	9.71
Difference	0.37	−0.55	0.06	−0.05	−0.17	0.13	−0.03	0.07	−0.01	0.16

	Empty APW sphere					Interstitial region
	s	p	d	f	Total	
Atomic superposed	0.33	0.16	0.21	0.00	0.70	2.53
Self-consistent	0.21	0.26	0.12	0.04	0.63	2.74
Difference	0.12	−0.10	0.09	−0.04	0.07	−0.21

Table 6. Theoretical and experimental results for the electron effective masses m_e^* and the hole effective masses m_h^* in Ag_2Te, measured in units of the free-electron mass m_0.

	Electrons, m_e^*/m_0		Holes, m_h^*/m_0	
Direction	Calculation	Experiment	Calculation	Experiment
Δ	0.034	——	0.5	——
Σ	0.039	——	2.0–3.6	——
Λ	0.043	——	0.9	——
Averaged	0.039	0.050–0.069 [19, 20]	1.3–2.1	1.0–2.0 [19, 40]

the three high-symmetry axes with $m_h^* = 2.1m_0$. Inclusion of the next lower p band reduces the hole effective mass from $2.1m_0$ to $1.3m_0$. These results are listed in table 6 together with the experimental values, which may be compared with the averaged theoretical values. We thus see that the magnitudes of both effective masses calculated for the Ag_2Te agree reasonably well with the experiments.

By means of elaborate electrical measurements on α-Ag_2Te, Miyatani [21] confirmed an appreciable deviation of the conduction band from a simple parabolic structure near the bottom, the Γ point. The non-parabolic effects are represented by the parameter β in the expression for the energy dispersion

$$E(k) = \frac{k^2}{m_e^*}\left\{1 - \beta\left(\frac{a_0}{2\pi}\right)^2 k^2\right\} \tag{3}$$

in atomic units. For $k \leqslant 0.05(2\pi/a_0)$, β is derived by means of a fitting to the numerical results along the three high-symmetry axes, and its mean value averaged over the three axes is $\beta = 92.6$ for the Ag_2Te. For a typical concentration of the electron carriers, 10^{19} cm^{-3}, the Fermi wave vector k_F takes a value of about $0.05(2\pi/a_0)$. The theoretical calculation predicts a value for β much larger than unity, which supports Miyatani's observation of $\beta = 17.5$. In contrast, the application of equation (3) to the FCC Te gives a negligible value for β, well below 10^{-2}. Note that equation (3) is valid for typical carrier densities; the non-parabolic term gives a contribution of 23% to $E(k)$ at $k_F = 0.05(2\pi/a_0)$.

Compared with the results for the FCC Te lattice, the doping of the Ag atoms into the

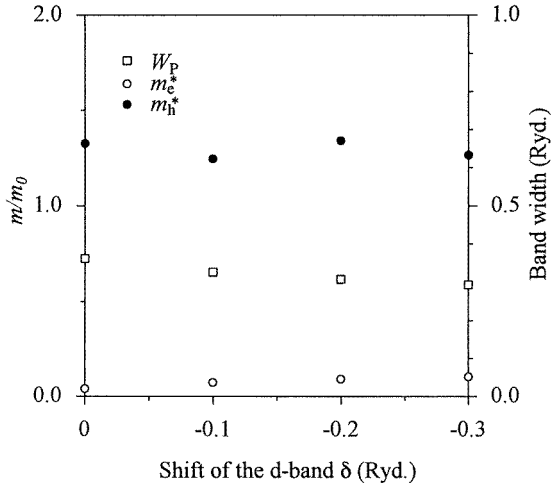

Figure 8. The dependence of the band-structure characteristics on the lowered shift δ of the Ag d band, where m_e^*, m_h^*, and W_p refer to the electron effective mass, the hole effective mass, and the width of the Te p band, respectively.

Te crystal is found to reduce the effective masses of both electrons and holes, and increase the non-parabolic coefficient β. The order-of-magnitude reduction of the electron effective mass, and the significantly non-parabolic form of the conduction band are explained by the strong hybridization of the Ag s state and the Te s state. The reduction of the hole effective mass and the accompanying increase of the p-band width, on the other hand, simply arise from the increase in the overlapping of the neighbouring Te p states due to the doping with Ag atoms; the Ag d states thus play no relevant roles. To demonstrate this fact, we took Li_2Te as a reference system. We note that Li_2Te has the same structure and a similar lattice constant to Ag_2Te, and that the Li atom has no d electrons. We iterated the band calculations for Li_2Te, and found the same effects on the valence band structure as were observed for Ag_2Te [38]. This picture is also supported by figure 8, which shows the dependence of the effective masses and the width of the Te p band on the selective shift of the Ag d band down to -0.3 Ryd. These band-structure characteristics are certainly not sensitive to the variation of the strength of the p–d hybridization.

3.4. Partial and total densities of states

The total density of states is calculated for the valence and the conduction bands as a function of energy. The result (solid curve) is shown in figure 9(a), where it is convoluted with a Lorentzian having a linewidth τ of 20 mRyd. The experimental density of states (dotted curve) observed by means of x-ray photoelectron spectroscopy [16] is also included. The small sharp peak that is located at around -0.52 Ryd originates from the Te 5s state. The large sharp peak that is located at around -0.08 Ryd originates from the Ag d bands, and its maximum value is 114 states Ryd^{-1}/cell. The broad peak that lies between the large sharp peak and E_F originates from the Te p bands. These results agree well with the experimental features measured by means of x-ray photoelectron spectroscopy. We thus find that the present model calculations are reasonably adaptable as regards predicting the electronic structure of α-Ag_2Te.

The total density of states can be decomposed into partial components according to the

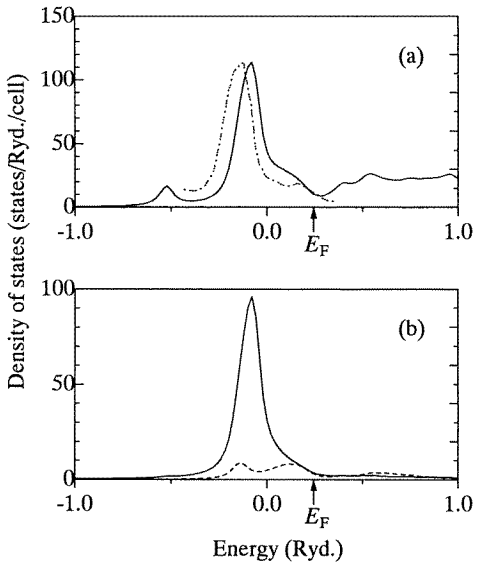

Figure 9. The total density of states (a) and the partial densities of states (b) calculated for Ag_2Te with the antifluorite structure. In panel (a), the solid curve shows the theoretical density of states, compared with x-ray photoelectron spectra (dotted curve) of the valence electrons of α-Ag_2Te; the maximum peak height in the experimental spectra is adjusted to that of the theoretical result. In panel (b), the solid and the dashed curves show the partial densities of states for the Ag d states and the Te p states, respectively. The theoretical densities of states are convoluted with a Lorentzian having a linewidth τ of 20 mRyd. E_F denotes the Fermi energy.

sites (the Te, Ag, empty APW spheres, and interstitial region) and the angular momenta (defined only in the APW spheres). Figure 9(b) shows the partial densities of states for the Ag d component (solid curve) and the Te p component (dashed curve). From the figure, the partial contributions due to Te p states and Ag d states overlap to an appreciable extent, as in the experimental observation for AgI. But the valence band generated by these overlapped states has already been shown not to be strongly hybridized.

4. Discussion

In order to approach the electronic structure of α-Ag_2Te, we have neglected the disordered and non-stoichiometric properties in the superionic conducting phase, and executed band-structure calculations for the hypothetical crystalline compound Ag_2Te. The ground-state properties so obtained agree well semiquantitatively with the experimental results, in view of the simplified computational model used.

The lattice constant of 6.576 Å measured for α-Ag_2Te is significantly smaller than the value that is expected from a simple ionic crystal model based on Pauling's ionic radius idea. That is, the ideal nearest-neighbour distance, given by addition of Pauling's ionic radii for Te and Ag ions, leads to a lattice constant of 8.014 Å for the Ag_2Te, which is much larger than both the calculated and measured results; in contrast, the same idea is highly applicable to the alkaline tellurides. We would like to emphasize here that the tendency towards such peculiar shrinking of α-Ag_2Te is reproduced by the energy band-structure calculation for the hypothetical crystalline compound. As regards the accuracy of the LAPW calculations applied to the corresponding alkaline tellurides, however, there remains a slight discrepancy

between the theoretical and experimental results; the accuracy is confirmed as within 1% for alkaline tellurides such as Li_2Te, Na_2Te, and K_2Te [45]. This discrepancy may be ascribed to the limitation of the LAPW calculation to the MTA in handling the fully occupied d states in Ag and/or the simplification of the present structure model for α-Ag_2Te.

Then, for the optimized parameters, which were defined so as to give a minimal total energy, the electronic energy band structure was calculated for the Ag_2Te compound with the antifluorite structure and the reference FCC Te system. The electronic properties such as the energy band gap and the effective masses obtained for the FCC Te cannot explain those observed for α-Ag_2Te. The discrepancies, can, however, be removed substantially by using the energy band structure calculated for the Ag_2Te; the addition of the Ag atoms into the FCC Te lattice affects the electronic structure drastically. In fact, the electronic structure obtained for the Ag_2Te is that of a narrow-gap semiconductor. Thus, the observed nature—that of a semiconductor with a narrow energy gap of order 0.007 Ryd (0.1eV)—can be understood semiquantitatively.

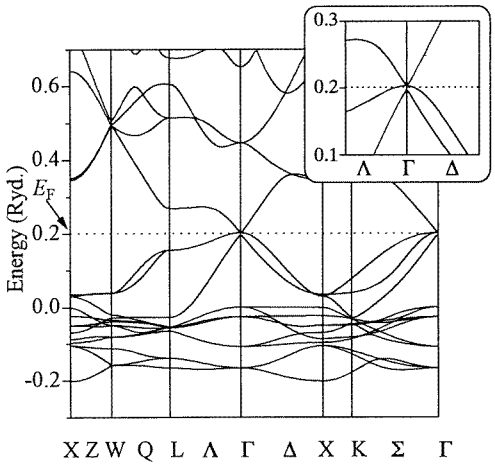

Figure 10. As figure 6, but calculated with *ad hoc* Kohn–Sham potentials obtained by superposing the atomic electron densities, and with APW spheres of identical radii. The inset is an enlargement of the band structure of metallic type in the vicinity of the Fermi level.

In a previous study [22] based on the APW method, the electronic band structure was metallic. The p–d hybridization thus had to be reduced through the selective shifting of the Ag d band to explain the semiconducting band structure of α-Ag_2Te; we have confirmed that the APW and LAPW calculations give the same result. This stands in sharp contrast with the present result, where the Ag_2Te is predicted to be a semiconductor without us having recourse to such artificial means. Figure 10 and figure 11, which should be compared with figure 6(a) in [22], show that the improvement can be traced back to the different choices of the APW sphere radii in the two calculations. Note that in the present calculation the empty spheres were placed at octahedral sites, unlike in the previous calculation. While the Ag d bands overlap the lower part of the Te p bands in the previous calculation with equal APW sphere radii, the Ag d bands are well separated from the Te p bands, and the semiconducting band structure materializes in the present calculation with the optimized APW sphere radii. We also note that the iterative procedure used to achieve self-consistency in the Kohn–Sham potentials tends to further localize the Ag d band, as can be appreciated by comparing figure 6 and figure 11.

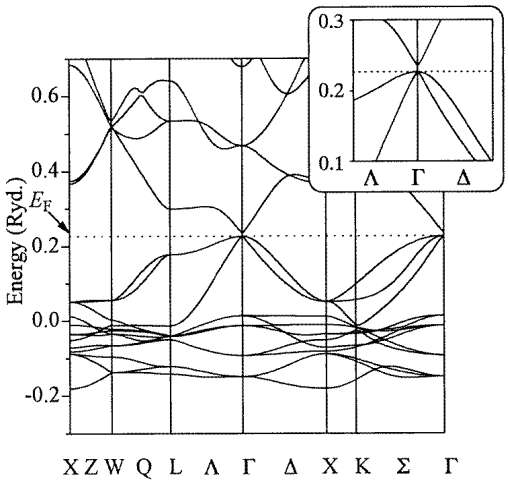

Figure 11. As figure 10, but calculated with APW spheres of optimized radii as used in figure 6. The inset is an enlargement of the band structure of semiconductor type in the vicinity of the energy gap.

As shown in table 3, the calculated band gap is somewhat larger than the experimental result. It is well known that the DFT calculations with the LDA tend to underestimate the band gaps for insulators [29, 35]. Since the band gap was measured at finite temperatures, it was possibly underestimated for such a narrow-gap semiconductor as α-Ag_2Te due to the thermal fluctuations. However, we do not stress the quantitatively excellent agreement as regards the energy band gap between the theoretical calculations and the experiments, considering the limitations of the LDA and the present structural model.

The present success in reproducing the electronic band structure in α-Ag_2Te even with the static model is clearly explained by this isolated nature of the Ag d band. The activation energy for the ionic diffusion in α-Ag_2Te, experimentally estimated as 0.007–0.015 Ryd (0.1–0.2 eV) [46], is much smaller than the shift of the Ag d band in figure 7. If the fast diffusion of Ag is stimulated by the p–d hybridization, it is reasonable to assume that possible shifts of the d bands due to the ionic motion are at most comparable to the activation energy. Moreover, the electrons in the lowest conduction band, predominantly composed of both Te and Ag s states, move throughout the crystalline compound. We therefore think that the disorder of Ag ions does not significantly affect the shape of the conduction band bottom. Combining these arguments with the results in figure 8, we infer that the ionic motion, taking place in the superionic phase, has no vital effect on the electronic band structure. To support this idea, we worked out a crystal structure with space group $F\bar{4}3m$ in which the Ag atoms are evenly distributed on the tetrahedral and octahedral sites, and carried out band calculations for the system imitating the disordered properties of the Ag ions. The x-ray diffraction measurements [23, 24] assigned 60–65% of the Ag ions to location around the 8c sites (tetrahedral sites) and the remainder to location around the 4b sites (octahedral sites) in α-Ag_2Te, assuming the crystal structure to have the space group $Fm3m$. The molecular dynamics calculations [43, 44] showed that the adjacent tetrahedral sites were connected through the octahedral sites in the diffusion process of the Ag ions. The structure with space group $F\bar{4}3m$ may indicate a greater degree of disorder of α-Ag_2Te than the experimental results for the statistical distribution of the Ag locations. The band calculations showed that such a scattered distribution of Ag exerted no significant influence

on the electronic structure, confirming the weak coupling between Ag d states and Te p states. Details of the calculation will be presented elsewhere [45]. Thus the superionic conductivity in α-Ag_2Te can hardly be ascribed to the p–d hybridization.

5. Concluding remarks

We have studied the ground-state properties and the electronic structure of α-Ag_2Te, by carrying out fully self-consistent LAPW calculations for a hypothetical crystalline compound, Ag_2Te with the antifluorite structure. The minimization procedure applied to the total energy reproduced the measured value for the lattice constant within an accuracy of 5%. The energy band structure so obtained at the equilibrium lattice constant was correctly predicted to be that of a narrow-gap semiconductor. The calculated effective masses of the electrons and holes were found to agree well quantitatively with the experimental results. The interrelationship between the Ag d band and Te p band was then elucidated, by demonstrating that these two bands were widely separated; the band-structure characteristics near the energy gap were not sensitive to the variation of the extent of the p–d hybridization. We therefore inferred that the p–d hybridization did not affect the ion dynamics in α-Ag_2Te strongly. Such a reduction of the p–d hybridization, which was required in the previous study to explain the semiconducting band structure for the α-Ag_2Te, has been naturally accounted for by imposing self-consistency on the theoretical calculations. We also found that the net charge contained in the APW spheres is considerably larger than the standard value for the effective charge of Ag ions used in molecular dynamics simulations.

Acknowledgments

We would like to thank Dr M Higuchi for useful discussions and helpful comments. The computational program used in this paper was developed on the basis of a LAPW code due to Professor S Asano. The numerical calculations were executed using the facilities of the Supercomputer Centre, Institute for Solid State Physics, University of Tokyo. This work was supported through a Grant-in-Aid for Scientific Research, provided by the Japanese Ministry of Education, Science and Culture. One of the authors (HI) appreciates financial support from the Uchida Science Foundation.

References

[1] Salamon M B 1979 *Physics of Superionic Conductors* (Berlin: Springer)
[2] Geller S 1977 *Solid Electrolytes* (Berlin: Springer)
[3] Subbarao E C 1980 *Solid Electrolytes and Their Applications* (New York: Plenum)
[4] Rickert H 1982 *Electrochemistry of Solids* (Berlin: Springer)
[5] Gurevich Y Y and Ivaov-Shits A K 1988 *Semiconductors and Semimetals* vol 26, ed R K Willardson and A C Beer (New York: Academic) p 229
[6] Tuller H L and Balkanski M 1989 *Science and Technology of Fast Ion Conductors* (New York: Plenum)
[7] Vashishta P, Mundy J N and Shenoy G K 1979 *Fast Ion Transport in Solids* (Amsterdam: North-Holland)
[8] Bates J B and Farrington G C 1981 *Fast Ion Transport in Solids* (Amsterdam: North-Holland)
[9] Kobayashi M 1990 *Solid State Ion.* **39** 121
[10] Williams D R, Jenkin J G, Leckey R C G and Liesegang J 1974 *Phys. Lett.* **49A** 141
[11] Bettini M, Suga S and Hanson R 1974 *Solid State Commun.* **15** 1885
[12] Goldman A 1977 *Phys. Status Solidi* b **81** 9
[13] Ostrow M and Goldman A 1979 *Phys. Status Solidi* b **95** 509
[14] Ves S, Glötzel D, Cardona M and Overhof H 1981 *Phys. Rev.* B **24** 3073
[15] Tejeda J, Shevchik N J, Braun W, Goldman A and Cardona M 1975 *Phys. Rev.* B **12** 1557

[16] Nemoshkalenko V V and Aleshin V G 1977 *Phys. Scr.* **16** 457
[17] Fedorin V A 1988 *Sov. Phys.–Solid State* **30** 76
[18] Rakitin A and Kobatashi M 1996 *Phys. Rev.* B **53** 3088
[19] Miyatani S 1958 *J. Phys. Soc. Japan* **13** 341
[20] Aliev S A and Agaev Z F 1983 *Izv. Akad. Nauk SSSR Neorg. Mater.* **19** 2050
[21] Miyatani S 1960 *J. Phys. Soc. Japan* **15** 1586
[22] Hasegawa A 1985 *Solid State Ion.* **15** 81
[23] Sakuma T and Saitoh S 1985 *J. Phys. Soc. Japan* **54** 3647
[24] Schneider J and Schulz H 1993 *Z. Kristallogr.* **203** 1
[25] Hohenberg K and Kohn W 1964 *Phys. Rev.* **136** B864
[26] Kohn W and Sham L J 1965 *Phys. Rev.* **140** A1133
[27] Kohn W and Vashishta P 1983 General density functional theory *Theory of the Inhomogeneous Electron Gas* ed S Lundqvist and N H March (New York: Plenum) p 79
[28] Jones R O and Gunnarsson O 1989 *Rev. Mod. Phys.* **61** 689
[29] Dreizler R M and Gross E K U 1990 *Density Functional Theory* (Berlin: Springer)
[30] Janak J F, Moruzzi V L and Williams A R 1975 *Phys. Rev.* B **12** 1257
[31] Koelling D D and Arbmann G O 1975 *J. Phys. F: Met. Phys.* **5** 2041
[32] Anderson O K 1975 *Phys. Rev.* B **12** 3060
[33] Takeda T and Kübler J 1979 *J. Phys. F: Met. Phys.* **9** 661
[34] Mattheiss L F, Wood J H and Switendick A C 1968 *Methods in Computational Physics* vol 8, ed B Alder, S Fernbach and M Rotenberg (New York: Academic) p 63
[35] Yin M T and Cohen M L 1982 *Phys. Rev.* B **26** 5668
[36] Onuki Y and Hasegawa A 1995 *Handbook on the Physics and Chemistry of Rare Earths* vol 20, ed K A Gschneidner Jr and L Eyring (Amsterdam: Elsevier) ch 135, p 1
[37] Glötzel D, Segall B and Anderson O K 1980 *Solid State Commun.* **36** 403
[38] Kikuchi H, Iyetomi H and Hasegawa A 1997 in preparation
[39] Honma K and Iida K 1987 *J. Phys. Soc. Japan* **56** 1828
[40] Aliev S A, Abdinov D Sh, Agaev Z F and Popov V V 1986 *Izv. Akad. Nauk SSSR Neorg. Mater.* **22** 757
[41] Murnaghan F D 1944 *Proc. Natl Acad. Sci. USA* **30** 244
[42] Berezin V M and Pashnin M I 1992 *Sov. Phys.–Solid State* **34** 162
[43] Tachibana F, Kobayashi M and Okazaki H 1989 *Phys. Rev.* B **40** 3360
[44] Tachibana F, Kobayashi M and Okazaki H 1988 *Solid State Ion.* **28–30** 41
[45] Kikuchi H, Iyetomi H and Hasegawa A 1997 in preparation
[46] Miyatani S 1981 *J. Phys. Soc. Japan* **50** 3415